Inorganic Chemistry

Article

pubs.acs.org/IC

Structure–Property Studies Toward the Stimuli-Responsive Behavior of Benzyl–Phospholium Acenes

Yi Ren and Thomas Baumgartner*

Department of Chemistry, University of Calgary, 2500 University Drive Northwest, Calgary, Alberta T2N 1N4, Canada

Supporting Information

ABSTRACT: A series of new phospholium acenes, quaternized with benzyl groups, was synthesized. Both different π-conjugated backbones and electron-donating/-withdrawing benzyl groups were systematically studied to reveal details on the nature of their structural dynamics. Extensive NMR studies (including variable concentration/temperature and 2D) suggested that the systems undergo *intramolecular* conformation changes in solution that are strongly affected by the electronic nature of the benzyl group, and thereby significantly affecting the phosphole-typical $\sigma^*-\pi^*$ interaction. This class of "smart" phosphole system exhibits enhanced emission in the solid state and at low temperature in solution, due to aggregation-induced enhanced emission (AIEE). The dynamic features of these smart phospholes also endow the systems with external-stimuli (thermal and mechanical force) responsive photophysical properties. Crystallographic studies and theoretical calculations confirmed that the thermal response of the phospholium system is mainly due to the conformation changes in solution, while the mechanical response of the system can be attributed to both the *intramolecular* conformation and the *intermolecular* organization changes in the solid state.

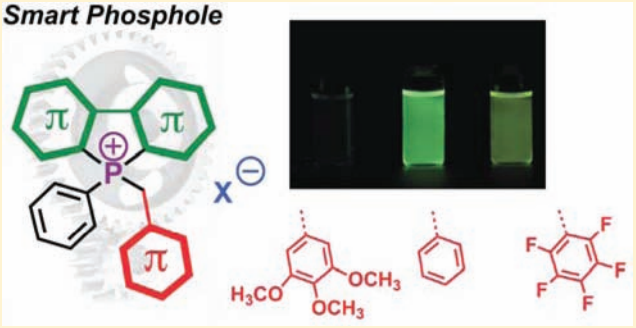

INTRODUCTION

Heteroatoms such as boron,[1] silicon,[2] phosphorus,[3] and sulfur[4] provide a variety of new and unique opportunities for tailoring the properties of π-conjugated systems including photophysics, solid organization, and electronics. Electronic doping using B,[5] Si,[6] P,[7] and/or S[8] heteroatoms (Chart 1) has thus been extensively studied in the context of organic functional materials for applications such as organic light-emitting diodes (OLEDs) and organic field-effect transistors (OFETs). The phosphole ring system in particular provides an intriguing perspective for organic electronics due to its intrinsically diverse and switchable chemistry involving both modification of the functional group E′ at phosphorus, via oxidation (S, O), borylation (BH_3), methylation (Me^+), and metalation (e.g., Au, Pd, Pt), as well as the electronic nature of the R groups[3] that can efficiently tune the properties of the systems (Chart 1, left).[7,9]

Chart 1. (Left) Phosphole-Based π-Conjugated Systems; (right, A) $n-\pi$ Orbital Coupling and (B) $\sigma^*-\pi^*$ Orbital Coupling of the Phosphole Systems

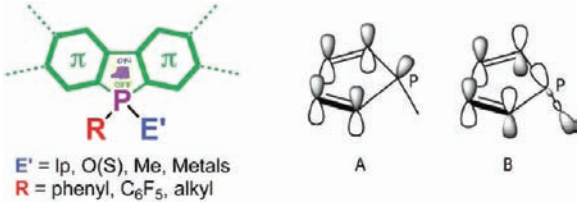

The most intriguing electronic features of phospholes are the hyperconjugation between the phosphorus lone pair with the π system (Chart 1A) as well as the coupling of the σ^* orbital of the exocyclic P–C bond with the endocyclic π^* system of the conjugated backbone (Chart 1B) that play a very important role for the electronic properties of such systems.[3,9] Instead of chemical modification of the phosphorus center, we envisioned that conformation changes of the phosphorus center may also be utilized to change the $\sigma^*-\pi^*$ orbital coupling. Moreover, the potential for addressing the photophysical properties of the systems via external stimuli (temperature and mechanical force) that trigger conformation changes may also exist. Recently, we were able to design a family of novel phosphole–lipids with dynamic features capable of inducing a variety of stimuli-responsive photophysical features and intriguing self-assembly properties (Chart 2, I).[10] In this contribution, we now report a series of model systems for these smart phospholes with both different π-conjugated backbones and contrasting electron-rich and electron-poor benzyl functionalization (Chart 2, II) to reveal more details on the recently discovered external-stimuli responsive behavior of the system. Our current systematic structural, photophysical, and theoretical studies unequivocally confirm that the electronic features of the benzyl substituents

Received: December 7, 2011
Published: January 27, 2012

   dx.doi.org/10.1021/ic2026335 | *Inorg. Chem.* 2012, 51, 2669–2678

Chart 2. Previously Reported Phosphole–Lipid Systems (I) and New Phospholium Model Species (II)

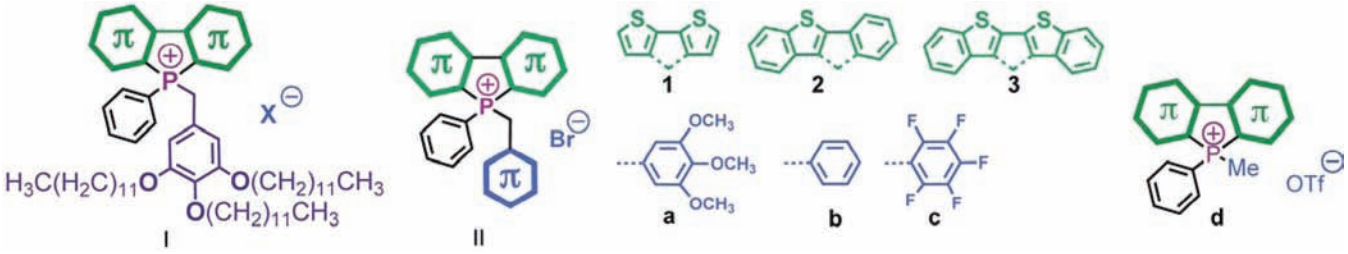

Table 1. Crystal Data and Structure Refinement for 1c, 3a, 3b, and 3c

	1c	3a	3b	3c
empirical formula	$C_{21}H_{11}F_5PS_2Br{\cdot}CHCl_3$	$C_{32}H_{26}O_3PS_2Br{\cdot}4CHCl_3$	$C_{29}H_{20}BrPS_2$	$C_{29}H_{15}F_5PS_2Br{\cdot}CHCl_3$
fw	652.67	1111.01	543.45	752.79
temp. (K)	173(2)	173(2)	173(2)	173(2)
wavelength (Å)	0.71073	0.71073	0.71073	0.71073
cryst syst	triclinic	triclinic	monoclinic	monoclinic
space group	*P*−1	*P*−1	*C*2/c	$P2_1/c$
a (Å)	10.0170(2)	13.9910(4)	25.0070(7)	13.0230(4)
b (Å)	11.6590(3)	14.0780(4)	9.9490(3)	13.9240(5)
c (Å)	12.7350(4)	14.3410(4)	19.5790(6)	20.6650(6)
α (deg)	68.464(2)	67.8960(10)	90	90
β (deg)	70.6040 (2)	62.2360(10)	93.640(2)	126.676(2)
γ (deg)	67.185(2)	84.393010)	90	90
vol. (Å)	1243.60(6)	2305.39(11)	4861.3(2)	3005.37(17)
Z	2	3	8	5
density, calcd (Mg/m^3)	1.743	1.600	1.485	1.664
abs coeff (mm^{-1})	2.256	1.747	1.945	1.879
F (000)	644	1112	2208	1496
cryst size (mm^{-3})	0.12 × 0.11 × 0.10	0.17 × 0.16 × 0.15	0.11 × 0.10 × 0.10	0.15 × 0.11 × 0.10
θ range (deg)	1.76–27.55	1.57–27.55	2.46–27.52	1.91–27.48
reflns collected	10 688	19 437	10 490	10 454
independent reflns	5686 (*R*(int) = 0.0285)	10 525 (*R*(int) = 0.0352)	5538 (*R*(int) = 0.0485)	6828 (*R*(int) = 0.0437)
data/restraints/params	5686/0/307	10 525/0/496	5538/0/298	6828/0/379
GoF on F^2	1.090	1.103	1.146	1.085
final *R* indices [$I > 2\sigma(I)$]	R_1 = 0.0416, wR_2 = 0.0828	R_1 = 0.0619, wR_2 = 0.1348	R_1 = 0.0546, wR_2 = 0.1317	R_1 = 0.0777, wR_2 = 0.1820
R indices (all data)	R_1 = 0.0552, wR_2 = 0.0947	R_1 = 0.0865, wR_2 = 0.1574	R_1 = 0.0777, wR_2 = 0.1459	R_1 = 0.1122, wR_2 = 0.2146

can effectively be used to manipulate the systems' properties without further chemical modification of the phosphorus center.

EXPERIMENTAL SECTION

General. All manipulations were carried out under a dry nitrogen atmosphere employing standard Schlenk techniques. Solvents were dried using an MBraun Solvent Purification System. Unless noted otherwise, starting materials were used as received. All trivalent phosphole compounds were synthesized according to our procedures reported before.[10] $^{31}P\{^1H\}$ NMR, ^1H NMR, and $^{13}C\{^1H\}$ NMR, and 2D NMR and variable-temperature ^1H NMR were recorded on Bruker DRX400 and Avance (-II,-III) 400 MHz spectrometers. Chemical shifts were referenced to external 85% H_3PO_4 (^{31}P) and external TMS (^{13}C, ^1H). Elemental analyses were performed in the Department of Chemistry at the University of Calgary. Mass spectra were run on a Finnigan SSQ 7000 spectrometer or a Bruker Daltonics AutoFlex III system. Thermal analyses were performed using a TA-Q200 DSC instrument. Crystal data and details of data collection are provided in Table 1 and the enclosed cif files, Supporting Information. Diffraction data were collected on a Nonius Kappa CCD diffractometer using Mo K*α* radiation (*λ*) 0.71073 Å (graphite monochromator). Structures were solved by direct methods (SHELXTL) and refined on F^2 by full-matrix least-squares techniques. All photophysical experiments were recorded in dichloromethane solution on a Jasco FP-6600 spectrofluorometer and UV–vis–NIR Cary 5000 spectrophotometer. Low-temperature fluorescence, fluorescence quantum yield, and lifetime were measured in dichloromethane solution using an Edinburgh Instruments Ltd. FLS920P fluorescence spectrometer equipped with an integrating sphere.

General Synthesis. Equimolar mixtures of the trivalent phospholes (**1**, **2**, **3**) and the corresponding benzyl bromide derivatives (**a**, **b**, **c**) in toluene/THF mixture were refluxed overnight. Subsequently, all solvents were removed under vacuum. The crude products were then washed with pentane and ethyl ether. The pure compounds were obtained by subsequent recrystallization from $CHCl_3$, CH_2Cl_2, or acetone. Note that the crystallized products commonly also capture solvents molecules. Dry products can be obtained after drying under vacuum.

Compound ***1a.*** ^1H NMR (600 MHz, $CDCl_3$): δ = 8.48–8.44 (m, 2H), 8.12 (dd, J = 5.04 Hz, J = 1.20 Hz, 2H), 7.73–7.69 (m, 1H), 7.64–7.62 (m, 2H), 7.53 (dd, J = 5.04 Hz, J = 4.14 Hz, 2H), 6.47 (d, J = 3.12 Hz, 2H), 5.22 (d, J = 14.94, 2H), 3.75 (s, 3H), 3.62 (s, 6H) ppm. $^{31}P\{^1H\}$ NMR (162 MHz, $CDCl_3$): 18.4 ppm. $^{13}C\{^1H\}$ NMR (100 MHz, $CDCl_3$): δ = 152.9 (d, J_{C-P} = 4.4 Hz), 149.4 (d, J_{C-P} = 18.8 Hz), 137.7 (d, J_{C-P} = 5.5 Hz), 134.9 (d, J_{C-P} = 3.2 Hz), 134.1 (d, J_{C-P} = 11.8 Hz), 130.4 (d, J_{C-P} = 15.4 Hz), 130.0 (d, J_{C-P} = 13.7 Hz), 129.2 (d, J_{C-P} = 14.3 Hz), 126.1 (d, J_{C-P} = 97.0 Hz), 121.1 (d, J_{C-P} = 10.0 Hz), 115.7 (d, J_{C-P} = 83.5 Hz), 107.5 (d, J_{C-P} = 6.2 Hz), 60.8 (s),

dx.doi.org/10.1021/ic2026335 | *Inorg. Chem.* 2012, 51, 2669–2678

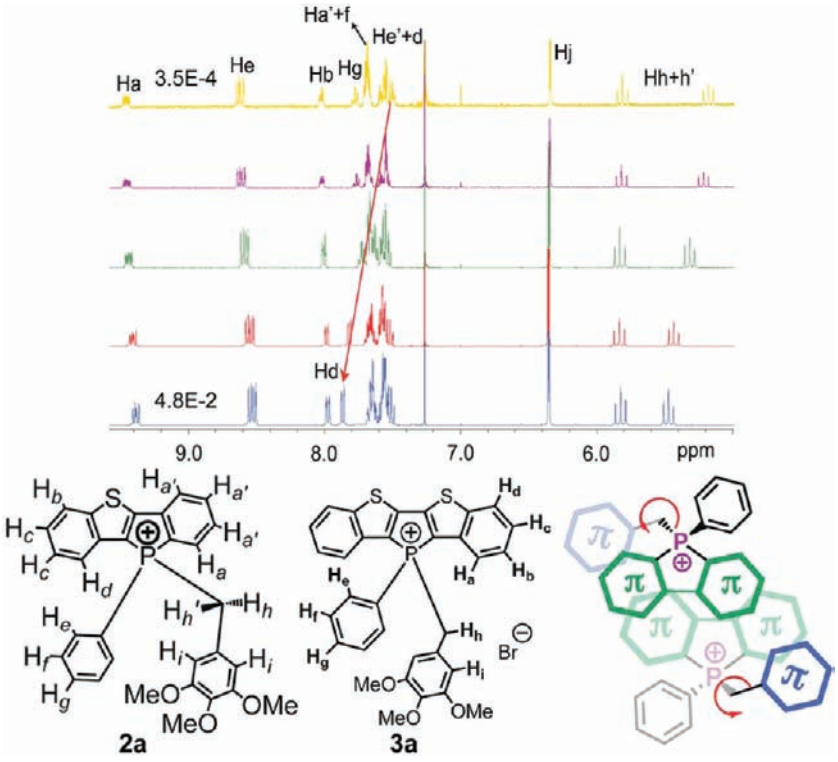

Figure 1. Plausible conformation changes in $CDCl_3$ at 298 K (low concentration, $\sim 10^{-4}$ M; high concentration, $\sim 10^{-2}$ M; arrow indicates Ar group leaving away from conjugated cores).

60.8 (s), 31.2 (d, J_{C-P} = 42.1 Hz) ppm. Anal. Calcd for $C_{21}H_{11}BrF_5PS_2$ (533.31): C, 54.04; H, 4.16. Found: C, 53.63; H, 3.99.

Compound ***1c***. ^{1}H NMR (400 MHz, $CDCl_3$): δ = 8.52−8.46 (m, 2H), 8.04 (dd, J = 4.80 Hz, J = 2.00 Hz, 2H), 7.81−7.76 (m, 2H), 7.71−7.65 (m, 1H), 7.58 (dd, J = 4.40 Hz, J = 5.20 Hz, 2H), 5.65 (d, J = 16.00 Hz, 2H) ppm. ^{31}P {^{1}H} NMR (162 MHz, $CDCl_3$): 15.0 (s br) ppm. ^{13}C{^{1}H} NMR (100 MHz, $CDCl_3$): δ = 149.7 (d, J_{C-P} = 20.4 Hz), 145.1 (dm, J_{C-F} = 258.4 Hz), 137.5 (dm, J_{C-F} = 257.6 Hz), 135.9 (d, J_{C-P} = 3.3 Hz), 134.0 (d, J_{C-P} = 12.4 Hz), 131.4 (d, J_{C-P} = 16.0 Hz), 130.4 (d, J_{C-P} = 14.2 Hz), 128.9 (d, J_{C-P} = 14.8 Hz), 125.0 (d, J_{C-P} = 97.4 Hz), 119.2 (dm, J_{C-F} = 208.8 Hz), 114.6 (d, J_{C-P} = 85.9 Hz) ppm. Anal. Calcd for $C_{21}H_{11}BrF_5PS_2{\cdot}CHCl_3$ (652.69): C, 40.48; H, 1.85. Found: C, 40.86; H, 1.34.

Compound ***2a***. ^{1}H NMR (400 MHz, $CDCl_3$): δ = 9.46−9.41 (m, 1H), 8.61−8.55 (m, 2H), 8.02−7.99 (m, 1H), 7.75−7.70 (m, 1H), 7.69−7.60 (m, 5H), 7.59−7.51 (m, 2H), 6.35 (d, J = 3.2 Hz, 2H), 5.83 (d, J = 15.2 Hz, 2H), 5.32 (d, J = 14.4 Hz), 3.67 (s, 3H), 3.28 (s, 3H) ppm. ^{31}P {^{1}H} NMR (162 MHz, $CDCl_3$): 25.9 ppm. ^{13}C{^{1}H} NMR (100 MHz, $CDCl_3$): δ = 160.4 (d, J_{C-P} = 21.7 Hz), 152.9 (d, J_{C-P} = 4.4 Hz), 142.9 (d, J_{C-P} = 13.1 Hz), 138.4 (d, J_{C-P} = 14.5 Hz), 137.6 (d, J_{C-P} = 5.0 Hz), 135.4 (d, J_{C-P} = 3.5 Hz), 135.3 (s), 135.2 (d, J_{C-P} = 2.0 Hz), 134.0 (d, J_{C-P} = 11.7 Hz), 131.2 (d, J_{C-P} = 12.3 Hz), 130.5 (d, J_{C-P} = 13.1 Hz), 127.5 (S), 126.8 (s), 126.1 (d, J_{C-P} = 91.8 Hz), 124.3 (s), 123.3 (s), 123.2 (d, J_{C-P} = 7.9 Hz), 116.1 (d, J_{C-P} = 81.7 Hz), 121.9 (d, J_{C-P} = 96.2 Hz), 107.4 (d, J_{C-P} = 5.8 Hz), 60.7 (s), 60.7 (s), 55.8 (s), 30.8 (d, J_{C-P} = 41.5 Hz) ppm. HRMS (MALDI-TOF): m/z = 463.0724 ([M − Br]$^+$, calcd 463.0739).

Compound ***2b***. ^{1}H NMR (400 MHz, $CDCl_3$): δ = 9.44−9.73 (m, 1H), 8.62−8.57 (m, 2H), 8.01−7.99 (m, 1H), 7.77−7.72 (m, 1H), 7.70−7.63 (m, 4H), 7.61−7.45 (m, 3H), 7.26 (d, J = 7.60 Hz, 1H,), 7.15−7.09 (m, 3H), 7.00 (t, J = 7.6 Hz, 2H), 5.58 (t, J = 15.2 Hz, 1H), 5.52 (t, J = 15.2 Hz, 1H) ppm. ^{31}P {^{1}H} NMR (162 MHz, $CDCl_3$): 25.8 ppm. ^{13}C{^{1}H} NMR (100 MHz, $CDCl_3$): δ = 160.5 (d, J_{C-P} = 22.5 Hz), 142.9 (d, J_{C-P} = 13.2 Hz), 138.0 (d, J_{C-P} = 15.1 Hz), 135.5 (d, J_{C-P} = 3.3 Hz), 135.4 (d, J_{C-P} = 11.3 Hz), 135.3 (d, J_{C-P} = 12.8 Hz), 135.1 (d, J_{C-P} = 2.0 Hz), 134.2 (d, J_{C-P} = 12.0 Hz), 131.5 (d, J_{C-P} = 12.4 Hz), 130.7 (s), 130.5 (d, J_{C-P} = 1.2 Hz), 130.5 (s), 128.8 (d, J_{C-P} = 3.9 Hz), 128.3 (d, J_{C-P} = 4.5 Hz), 127.4 (S), 126.8 (s), 126.8 (d, J_{C-P} = 11.5 Hz),126.3 (d, J_{C-P} = 91.2 Hz), 124.3 (s), 123.1 (s), 123.0 (d, J_{C-P} = 8.3 Hz), 115.8 (d, J_{C-P} = 82.1 Hz), 114.6 (d, J_{C-P} = 95.3 Hz), 30.9 (d, J_{C-P} = 41.9 Hz) ppm. Anal. Calcd for $C_{27}H_{20}BrPS$ (487.39): C, 66.54; H, 4.14. Found: C, 66.17; H, 3.97.

Compound ***2c***. ^{1}H NMR (400 MHz, $CDCl_3$): δ = 9.82−9.23 (m, 1H), 8.64−8.58 (m, 2H), 8.03−8.58 (m, 1H), 8.03−8.00 (m, 2H), 7.74−7.68 (m, 4H), 7.57−7.48 (m, 2H), 7.40 (d bro, J = 8.0 Hz, 1H), 6.02 (t bro, J = 15.6 Hz, 1H), 5.74 (t bro, J = 15.6 Hz, 1H) ppm. ^{31}P {^{1}H} NMR (162 MHz, $CDCl_3$): 22.3 (s, br) ppm. ^{13}C{^{1}H} NMR (100 MHz, $CDCl_3$): δ = 161.0 (d, J_{C-P} = 23.2 Hz), 145.4 (d bro, J_{C-P} = 258.1 Hz), 142.9 (d, J_{C-P} = 13.2 Hz), 137.9 (d, J_{C-P} = 16.1 Hz), 136.2 (d, J_{C-P} = 3.4 Hz), 136.0 (d, J_{C-P} = 2.2 Hz), 135.5 (d, J_{C-P} = 11.5 Hz), 134.7 (d, J_{C-P} = 12.7 Hz), 134.2 (d, J_{C-P} = 12.6 Hz), 131.9 (d, J_{C-P} = 12.5 Hz), 130.8 (d, J_{C-P} = 13.9 Hz), 127.6 (s), 127.2 (s), 125.7 (d, J_{C-P} = 91.7 Hz), 124.5 (s), 123.4 (d, J_{C-P} = 8.7 Hz), 122.4 (s), 114.6 (d, J_{C-P} = 83.5 Hz), 20.8 (d, J_{C-P} = 47.3 Hz) ppm. HRMS (MALDI-TOF): m/z = 497.0544 ([M − Br]$^+$, calcd 497.0547).

Compound ***3a***. ^{1}H NMR (400 MHz, $CDCl_3$): δ = 8.74−8.68 (m, 2H), 8.30 (d bro, J = 8.0 Hz, 2H), 7.96 (d br, J = 8.4 Hz, 2H), 7.81−7.77 (m, 1H), 7.73 − 7.65 (m, 4H), 7.54−7.50 (m, 2H), 6.33 (d, J = 3.2 Hz, 2H), 5.73 (d, J = 13.2 Hz, 2H), 3.67 (s, 3H), 3.18 (s, 6H) ppm. ^{31}P {^{1}H} NMR (162 MHz, $CDCl_3$): 21.4 ppm. ^{13}C{^{1}H} NMR (100 MHz, $CDCl_3$): δ = 153.0 (d, J_{C-P} = 4.4 Hz), 150.8 (d, J_{C-P} = 18.3 Hz), 143.0 (d, J_{C-P} = 13.8 Hz), 137.7 (d, J_{C-P} = 2.4 Hz), 135.9 (d, J_{C-P} = 3.1 Hz), 135.0 (d, J_{C-P} 13.5 Hz), 134.2 (d, J_{C-P} = 12.4 Hz), 130.9 (d, J_{C-P} = 13.7 Hz), 128.2 (s), 127.0 (s), 124.3 (s), 123.9 (s), 121.5 (d, J_{C-P} = 95.4 Hz), 121.5 (d, J_{C-P} = 9.9 Hz), 114.4 (d, J_{C-P} = 81.4 Hz), 107.4 (d, J_{C-P} = 6.2 Hz), 60.7 (s), 60.7 (s), 55.6 (s), 29.7 (d, J_{C-P} = 41.3 Hz) ppm. Anal. Calcd for $C_{32}H_{26}BrO_3PS_2$ (633.55): C, 60.66; H, 4.14. Found: C, 60.21; H, 4.24.

Compound ***3b***. ^{1}H NMR (400 MHz, $CDCl_3$): δ = 8.72−8.66 (m, 2H), 8.10 (d br, J = 7.6 Hz, 2H), 7.96 (d br, J = 8.4 Hz, 2H), 7.81−7.76 (m, 1H), 7.73−7.68 (m, 2H), 7.64−7.60 (m, 2H), 7.54−7.50 (m, 2H), 7.16−7.08 (m, 3H), 7.01 (m, 2H), 5.76 (d, J = 14.0 Hz, 2H) ppm. ^{31}P {^{1}H} NMR (162 MHz, $CDCl_3$): 21.4 ppm. ^{13}C{^{1}H} NMR (100 MHz, $CDCl_3$): δ = 143.0 (d, J_{C-P} = 14.2 Hz), 135.9 (d, J_{C-P} =

dx.doi.org/10.1021/ic2026335 | *Inorg. Chem.* 2012, 51, 2669−2678

3.2 Hz), 135.0 (d, J_{C-P} = 13.3 Hz), 134.3 (d, J_{C-P} = 12.5 Hz), 131.0 (d, J_{C-P} = 13.7 Hz), 130.5 (d, J_{C-P} = 6.3 Hz), 128.9 (d, J_{C-P} = 4.0 Hz), 128.5 (d, J_{C-P} = 13.7 Hz), 128.2 (s), 127.1 (s), 126.5 (d, J_{C-P} = 9.6 Hz), 124.1 (s), 123.9 (s), 29.8 (d, J_{C-P} = 41.5 Hz) ppm. HRMS (MALDI-TOF): m/z = 463.0724 ([M − Br]$^+$, calcd 463.0739).

Compound ***3c***. ^{1}H NMR (400 MHz, $CDCl_3$): δ = 8.72−8.65 (m, 2H), 8.25 (d br, J = 8.0 Hz, 2H), 8.01−7.98 (m, 2H), 7.86−7.81 (m, 1H), 7.77−7.61 (m, 2H), 7.69−7.65 (m, 2H), 7.58−7.54 (m, 2H), 6.18 (d, J = 14.8 Hz, 2H) ppm. ^{31}P {^{1}H} NMR (162 MHz, $CDCl_3$): 16.8 (s, br) ppm. ^{13}C{^{1}H} NMR (100 MHz, $CDCl_3$): δ = 151.3 (d, J_{C-P} = 19.6 Hz), 143.1 (d, J_{C-P} = 14.3 Hz), 136.6 (d, J_{C-P} = 3.2 Hz), 134.6 (d, J_{C-P} = 14.2 Hz), 134.2 (d, J_{C-P} = 13.0 Hz), 131.2 (d, J_{C-P} = 14.3 Hz), 128.4 (s), 127.4 (s), 124.1 (s), 123.7 (s), 119.9 (d, J_{C-P} = 95.7 Hz), 113.2 (d, J_{C-P} = 84.2 Hz), 19.6 (d, J_{C-P} = 46.3 Hz) ppm. Anal. Calcd. for $C_{30}H_{76}BrCl_3F_5PS_2{\cdot}CHCl_3$ (752.81): C, 47.86; H, 2.14. Found: C, 48.22; H, 2.15.

RESULTS AND DISCUSSION

Synthesis and Conformation Studies. Synthesis of the new phospholium compounds was adopted from our earlier studies involving efficient quaterization of the trivalent phosphorus center in the respective conjugated ring-fused phospholes with the corresponding benzyl bromides.[10] The different conjugated backbones and substituted benzyl groups were used to systematically investigate their effects on the geometric parameters and electronic features of the systems. The identity of all new phospholium acenes was confirmed by multinuclear (^{1}H, ^{13}C, and ^{31}P) NMR spectroscopy, high-resolution mass spectrometry, and elemental analysis.

In analogy to our initial work on the phosphole−lipid system, variable-concentration (^{1}H, ^{31}P, and 2D) NMR studies (10^{-4}−10^{-2} M, Figure 1 and Supporting Information) of the compounds with the trimethoxybenzyl and benzyl groups (**1a**,**b** **2a**,**b**, and **3a**) revealed a noticeable *intramolecular* conformation change with the benzyl group being pushed away from the conjugated backbone through *intermolecular* interactions (ionic, H−π, and π−π; see Supporting Information).[11] As seen in Figure 1, H_d of **2a** shows a significant downfield shift (ca. 0.3 ppm) supporting the deshielding effect of the leaving benzyl group upon increasing the concentration from 3.46 × 10^{-4} to 4.81 × 10^{-2} M. In addition, the chemical shift changes of H_h and $H_{h'}$ also support rotation of the P−C_{benzyl} bond. It is worth mentioning that H_i of **2a** and H_a of **3a** exhibit interactions with H_d and H_e in the ^{1}H−^{1}H NOESY spectrum (see Supporting Information) at both lower (10^{-3} M) and higher concentrations (10^{-5} M), which is different from the related tridodecyloxy−phospholium derivative reported before.[10] Such difference could be rationalized by the less bulky trimethoxybenzyl group of **2a** being located closer to the conjugated backbone. In contrast to the electron-donating benzyl group, **1c** and **2c** with the electron-poor pentafluorobenzyl group only exhibit a small change in their ^{1}H and ^{31}P chemical shifts (see Supporting Information),[11] thereby supporting a more rigid structure in the latter case, which can be attributed to different electrostatic interactions between the conjugated cores and the various benzyl moieties (electron donating or withdrawing); variable-temperature NMR experiments further support the differences in the dynamic features of these compounds (see Supporting Information). Clearly, systematic NMR studies confirm that the dynamic structural features of the new phospholium systems are effectively controlled by the electronic nature of substituted benzyl group and its electrostatic interactions with the conjugated acene scaffold.

In addition, we were able to crystallize **1a**,**c**, **2b**,**c**, and **3a**−**c** from different organic solvents (Figures 2−5).[12] The new

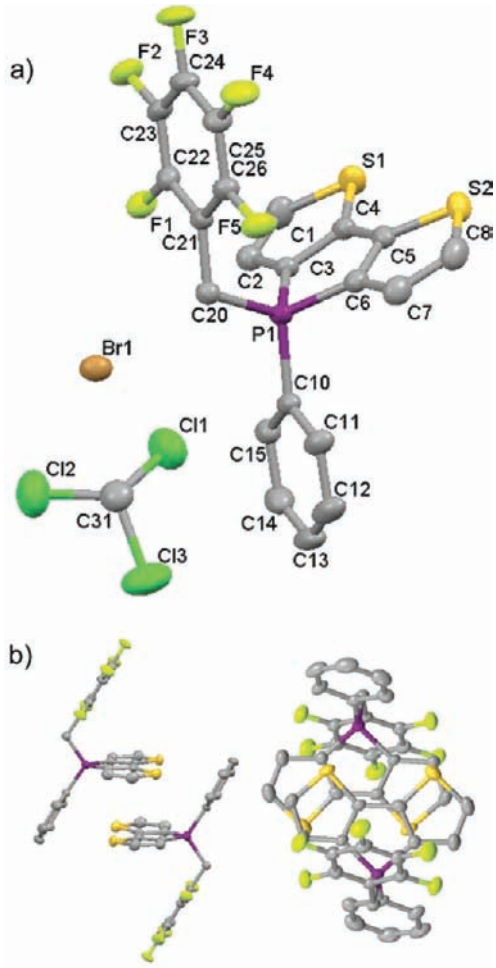

Figure 2. (a) Molecular structure of **1c** in the solid state (50% probability level; hydrogen atoms omitted for clarity). Selected bond lengths [Angstroms] and angles [degrees]: P1−C3, 1.778(3); P1−C6, 1.776(3); P1−C10, 1.792(3); P1−C20, 1.804(3); C20−C21, 1.506(4); C3−C4, 1.384(4); C4−C5: 1.454(4); C5−C6, 1.386(4); C3−P1−C6, 94.50(14); C3−P1−C10, 113.16(12); C6−P1−C10, 110.98(15); C21−C20−P1, 112.5(12). (b) Molecular packing of **1c** (50% probability level; solvent molecule and hydrogen atoms omitted for clarity).

phospholium compounds have similar structures to the corresponding methyl phospholium derivatives reported before (**1d**, **2d**, and **3d**).[9a,e,f] Due to the expected correlation between the environment of the phosphorus center and the σ^*−π^* orbital coupling, the geometry around phosphorus was considered to be an excellent indicator for this purpose. The sum of the angles around phosphorus (based on the two endocyclic phosphole P−C bonds and the exocyclic P−C_{Ph} bond) was found to be highly dependent on the electronic nature of the benzyl groups (**3a**, 316.8°; **3b**, 317.7°; **3c**, 322.9°; cf. **3d**, 317.4° and **1c**, 318.6°, cf. **1d**, 317.7°), indicating that the benzyl group has a comparatively strong effect on the geometry of the phosphorus center.[9e,f] As reported before in this context, we could obtain two different isomers of **1b** ("open form" and "closed form") from slow evaporation of the different solvents that support the structural flexibility of the benzyl group in

dx.doi.org/10.1021/ic2026335 | Inorg. Chem. 2012, 51, 2669−2678

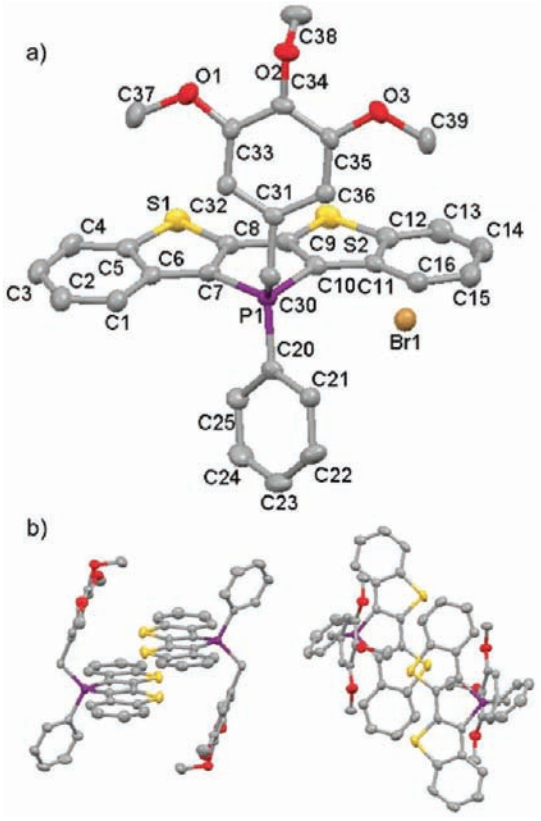

Figure 3. (a) Molecular structure of **3a** in the solid state (50% probability level; solvent molecules and hydrogen atoms omitted for clarity). Selected bond lengths [Angstroms] and angles [degrees]: P1–C7, 1.788(4); P1–C10, 1.794(4); P1–C20, 1.783(4); P1–C30, 1.799(4); C30–C31, 1.509(6); C7–C8, 1.372(6); C8–C9, 1.451(6); C9–C10, 1.373(6); C7–P1–C10, 93.8(2); C7–P1–C20, 111.7(2); C10–P1–C20, 111.3(1); C31–C30–P1, 114.7(3). (b) Molecular packing of **3a** (50% probability level; solvent molecules and hydrogen atoms omitted for clarity).

general (Figure 6).[10] Importantly, the sum of the angles around phosphorus is also a direct result of these conformations of **1b** (**1b**-*open*, 321.0°; **1b**-*closed*, 316.0°). Besides, the **1b**-*open* isomer exhibits better $\pi-\pi$-stacking interactions (Figure 6b). Compared to the methyl phospholium derivatives **2d** and **3d**,[9a,f] dimer-like structures could only be observed in **3a**, **3b**, and **3c**, however, with less efficient $\pi-\pi$ stacking, which is likely due to the bulkier benzyl group reducing the long-range intermolecular interactions (Figures 3b, 4b, and 5b).

Compound **3c** with the perfluorinated benzyl group shows better $\pi-\pi$ stacking (3.49 Å, Figure 5b) with the benzannelated thieno moieties of two adjacent molecules partially overlapping. By contrast, the trimethoxybenzyl (**3a**, Figure 3b) and benzyl (**3b**, Figure 4b) varieties only show a small overlap of their thieno moieties. The main reason for this observation seems to be the steric bulk of the trimethoxybenzyl groups that prevents strong $\pi-\pi$ stacking, while the electron-withdrawing pentafluorobenzyl group decreases the electron density of the conjugated backbones that consequently induces stronger $\pi-\pi$-stacking interactions. This hypothesis is further supported by **1c** with the smaller conjugated backbone, displaying even better $\pi-\pi$ overlap between the dimers (Figure 2b, 3.67 Å) than the extended relatives such as **3a** and **3b**, which is also supported by a more red-shifted solid-state fluorescence emission (powder and crystal) of **1c** compared to its solution (vide infra).

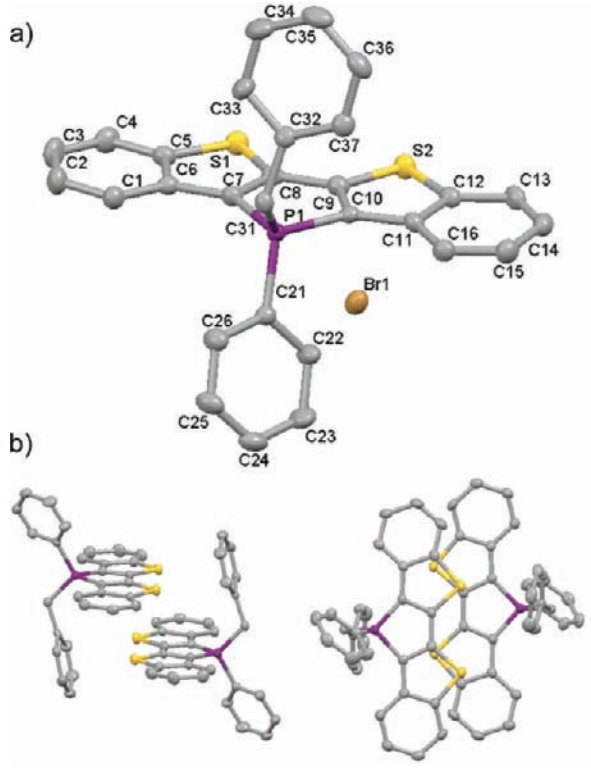

Figure 4. (a) Molecular structure of **3b** in the solid state (50% probability level; hydrogen atoms omitted for clarity). Selected bond lengths [Angstroms] and angles [degrees]: P1–C7, 1.791(4); P1–C10, 1.788(4); P1–C21, 1.797(4); P1–C31, 1.794(4); C31–C32, 1.514(5); C7–C8, 1.378(6); C8–C9, 1.456(6); C9–C10, 1.364(5); C7–P1–C10, 93.59(18); C7–P1–C21, 113.85(18); C10–P1–C21, 110.28(18); C32–C31–P1, 116.81(3). (b) Molecular packing of **3b** (50% probability level; hydrogen atoms omitted for clarity).

Photophysical Properties. The photophysical properties of the new systems that were also found to be highly dependent on the electronic nature of the benzyl groups are summarized in Table 2. Generally, the electronic nature of the benzyl groups does essentially not affect the absorption wavelengths of the compounds in solution within each of the series **1**, **2**, or **3** (Figure 7a). However, the emission properties indeed show a dependence on the electronic nature of the benzyl groups with the electron-poor perfluorinated benzyl group inducing the strongest red shift in CH_2Cl_2 with the general trend λ_{em} **c** > **b** > **a** (Figure 7a). These observations suggest that the phospholium systems with the electron-poor pentafluorobenzyl group have a more polar excited state compared to the respective ground state, which likely also involves a considerably changed $\sigma^*-\pi^*$ interaction.[3] It should be mentioned that **1c** exhibits a blue-shifted emission compared with its nonfluorinated congener **1b**. Although the exact reason for this observation is not clear at this stage, this feature can likely be attributed to a different excited state of **1c**, induced by the electron-withdrawing nature of the perfluorinated benzyl group.

Compared to the known methyl phospholium derivatives (**1d**, 0.53; **2d**, 0.36; **3d**, 0.31),[9a,e,f] the benzyl-substituted phospholium species generally show lower fluorescence quantum yields in solution (Table 2) that can be attributed to the flexibility of the benzyl groups as confirmed with the (variable-concentration/temperature) NMR studies (vide supra). Compounds **1a**, **2a**, and **3a** with the electron-rich trimethoxybenzyl group exhibit relatively low quantum yields in

dx.doi.org/10.1021/ic2026335 | *Inorg. Chem.* 2012, 51, 2669–2678

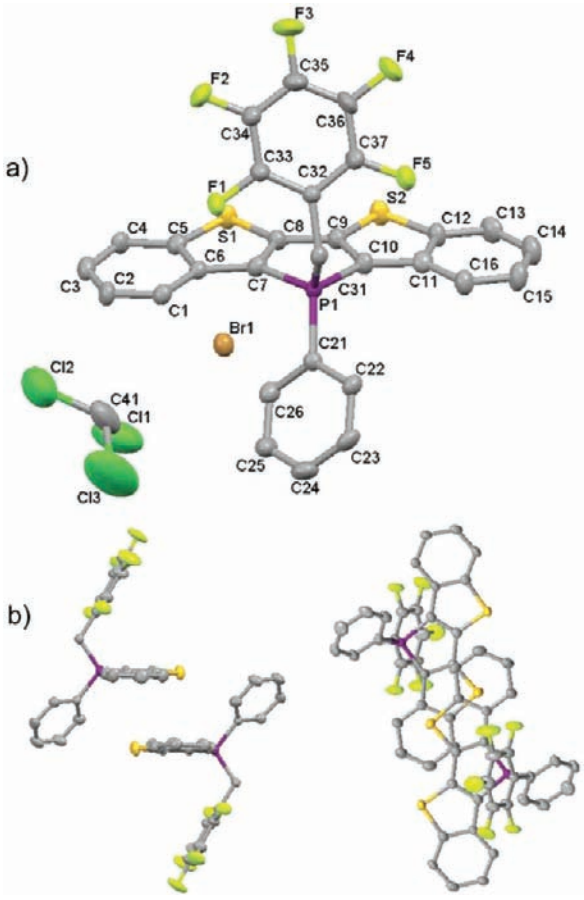

Figure 5. (a) Molecular structure of **3c** in the solid state (50% probability level; hydrogen atoms omitted for clarity). Selected bond lengths [Angstroms] and angles [degrees]: P1−C7, 1.787(6); P1−C10, 1.787(6); P1−C21, 1.790(6); P1−C31, 1.803(6); C31−C32, 1.508(7); C7−C8, 1.367(8); C8−C9, 1.458(8); C9−C10, 1.376(8); C7−P1−C10, 94.1(3); C7−P1−C21, 112.1(3); C10−P1−C21, 116.7(3); C32−C31−P1, 113.5(4). (b) Molecular packing of **3c** (50% probability level; solvent molecule and hydrogen atoms omitted for clarity).

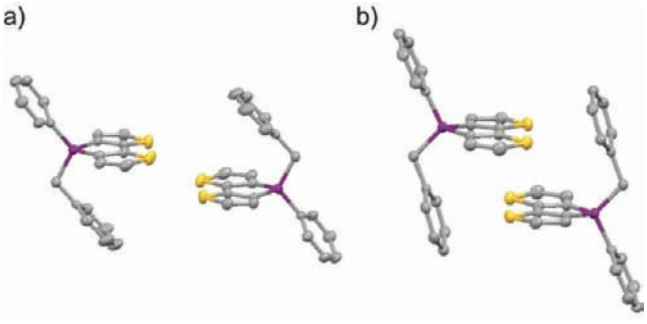

Figure 6. Molecular packing of **1b**: (a) **1b**-*closed* and (b) **1b**-*open* (a solvent molecule, counteranion, and hydrogen atoms omitted for clarity).[10]

solution (**1a**, ϕ = 0.03; **2a**, ϕ = 0.04; **3a**, ϕ = 0.06), indicating that a photoinduced electron transfer (PET) from the trimethoxyphenyl donor moiety to the conjugated phospholium acceptor (Figure 7b) could be an additional nonradiative channel next to intramolecular rotation (IMR), similar to the properties of the related phosphole−lipids.[10] Notably, the photoluminescence quantum yields commonly increase from the **a**-, to the **b**, to the **c** series (with **3b** and **3c** showing values as high as ϕ = 0.38 and 0.44 in solution, respectively), reflecting the donor capability (or lack thereof) of the benzyl group that is necessary to induce the PET. It is important to note that all compounds exhibit higher fluorescence quantum yields in the solid state (**1a**, 4.7 times; **1b**, 10 times; **1c**, 1.2 times; **2a**, 1.5 times; **2b**, 2 times; **2c**, 1.3 times; **3a**, 2.2 times; **3b**, 2.2 times; **1a**, 1.6 times) due to aggregation-induced enhanced emission (AIEE) likely resulting from the restricted intramolecular rotation (IMR) of the benzyl groups (Figure 7b).[9a,e,f,13] Remarkably, **3b** and **3c** with a larger conjugated core show surprisingly high quantum yields (ca. 80%) in the solid state by taking advantage of the bulky phospholium center that prevents fluorescence quenching through aggregation (vide supra).[14]

The dynamics of the benzylated phospholium center endow the systems with very interesting photophysics that are distinctly different from the known dithienophosphole derivatives (Figure 8a and 8b).[9] First, compounds with the electron-rich trimethoxyphenyl group exhibit a more red-shifted solid-state emission (powder and crystal) compared to their solutions (**1a**, $\Delta\lambda_{em}$ = 17 nm; **2a**, $\Delta\lambda_{em}$ = 22 nm; **3a**, $\Delta\lambda_{em}$ = 29 nm). On the basis of the solid-state structures and theoretical calculations using π-stacked dimers of **1a** and **3a** (vide infra) this stronger red-shifted solid-state emission can be attributed to an intermolecular charge transfer from the electron-rich trimethoxybenzyl group (HOMO) to the π-conjugated cores of a neighboring molecule (LUMO). In stark contrast, **2c** and **3c** with the electron-poor pentafluorobenzyl ring exhibit a blue-shifted emission in their powder state compared to their solutions. Due to the steric bulk around the phosphorus center, H-aggregation can be ruled out for these phospholium systems. Considering that J-aggregation usually induces red-shifted emission features in the solid state, such blue-shifted emission can only be explained by different *molecular* conformations in the solid state and solution, respectively. As already mentioned, **1c** with the small conjugated backbone shows a significant red-shifted emission compared to its solution, likely due to excimer formation, which correlates well with effective intermolecular π-stacking interactions observed in the X-ray diffraction study of **1c**. Second, the solution emission spectra of the **1**, **2**, and **3** series are generally much broader than those of the corresponding solids, suggesting the existence of different isomers in solution as a result of the flexible structures (Figure 8c and Supporting Information). Finally, the emissions of the corresponding single crystals (**1a−c**, **2b**,**c**, and **3a−c**) are also different from those in solution and the solid powders (Figure 8a, and Supporting Information). More importantly, as observed previously, the **1b**-*open* isomer exhibits a 9 nm red-shifted solid-state emission compared with the **1b**-*closed* isomer (Figure 8b), which further supports our hypothesis of conformation-dependent emission features.

Stimuli-Responsive Studies. On the basis of our initial study and further solidifed by this work, the dynamic structural features offer the system with intriguing thermally responsive photophysics that are highly dependent on both the electronic nature of the benzyl ring and the conjugated backbones. As shown in Figure 9a, compounds **1a** and **3a** with the electron-rich trimethoxyphenyl group show the most significant hyperchromic shift (**1a**, 24 times; **3a**, 8 times), and **1a**, **2a**, and **3a** exhibit the most red-shifted emission (**1a**, $\Delta\lambda_{em}$ = 6 nm; **2a**, $\Delta\lambda_{em}$ = 13 nm; **3a**, $\Delta\lambda_{em}$ = 16 nm) in CH_2Cl_2 (10^{-5} M, Figure 8a and 8b) compared with the other compounds in the same series upon decreasing the temperature from room

dx.doi.org/10.1021/ic2026335 | *Inorg. Chem.* 2012, 51, 2669−2678

Table 2. Photophysical Properties of the 1, 2, and 3 Series

compd	λ_{abs} [nm] (CH_2Cl_2)	ε^a [L·mol^{-1}·cm^{-1}]	λ_{em} [nm] (CH_2Cl_2)	λ_{em} [nm] (solid)	λ_{em} [nm] (crystal)	λ_{em} [nm] (AS^b)	$\phi_{PL}{}^c$ (CH_2Cl_2)	$\phi_{PL}{}^c$ (solid powder)
1a	372	8300	450	467	461 ($CHCl_3$)^d	NA	0.03	0.14
					472 (EA)^e	469		
1b	372	6384	463	466	456 (DCM)^d	453	0.060	0.60
					465 ($CHCl_3$)^d	462		
1c	376	8987	453	469	476 ($CHCl_3$)^d	474	0.12	0.14
2a	337	7853	424	446	NA	NA	0.04	0.06
2b	337	10 134	442	446	445	441	0.18	0.36
2c	340	9642	452	443	444	442	0.18	0.23
3a	417	11 285	500	529	523 ($CHCl_3$)^d	521	0.06	0.13
3b	419	17 065	516	516	526	515	0.36	0.80
3c	425	16 554	528	525	533 ($CHCl_3$)^d	522	0.49	0.77

$^a\varepsilon$: molar absorption coefficient. ^{b}After shearing. ^{c}Fluorescence quantum yield was determined by a calibrated integrating sphere system. ^{d}Solvents that cocrystallized with the compounds. ^{e}Crystal obtained from slow evaporation of ethyl acetate (EA).

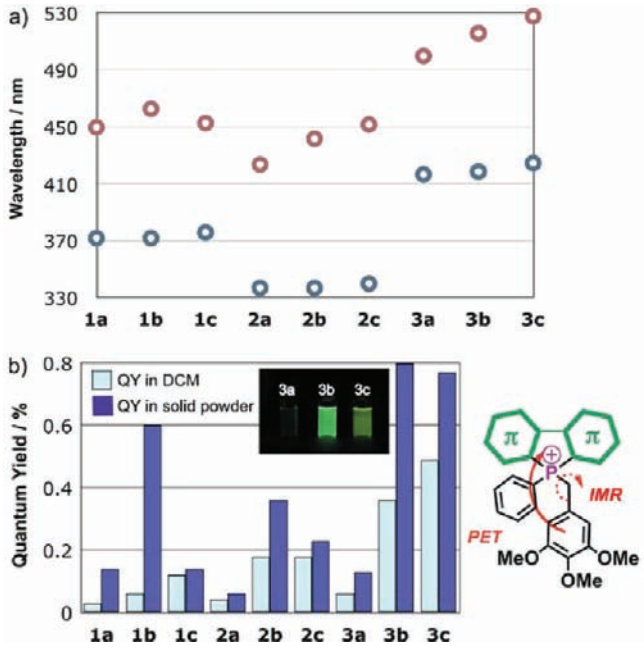

Figure 7. (a) Absorption and emission wavelengths of the **1**, **2**, and **3** series. (b) Quantum yields of the compounds in solution and the solid state (PET = photoinduced electron transfer; IMR = intramolecular rotation).

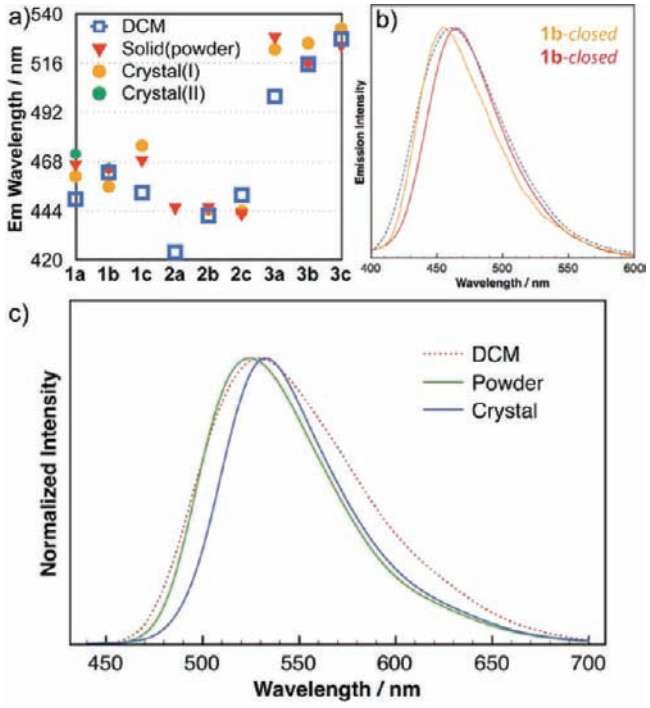

Figure 8. (a) Emission properties of the **1**, **2**. and **3** series. (b) Normalized emission spectra of **3c** under different conditions.

temperature to −60 °C. These observations suggest that the stronger electon-donating character of the trimethoxybenzyl group leads to a more flexible structure than in the other systems (vide supra) due to both the steric demand and the electronic repulsion of the trimethoxybenzyl group. The weak hyperchromic shift of **2a** is likely due to different conformations that change the distance between the trimethoxybenzyl group and conjugated cores and the underlying flexibity of the structure that affects the nonradiative decay processes (PET or IMR) and the emission intensity. Besides, the **1** series with the smaller conjugated backbone exhibits a more enhanced emission at low temperature than the **2** and **3** series with extended conjugated backbones. It is likely that the smaller conjugated backbone, with decreased potential of intramolecular benzyl/π-scaffold interaction, endows the **1** series with a generally more flexible structure. Remarkably, the thermally responsive hyperchromic shift and red-shifted emission are comparable to the chemical modification of the phosphorus center of the corresponding systems reported before.[9] Variable-temperature (VT) ^{1}H NMR (CD_2Cl_2) suggests that the benzyl rings approach the conjugated cores more closely upon decreasing the temperature (see Supporting Information). The VT ^{31}P NMR experiments further support the change of the phosphorus environment in the systems. Therefore, it is believed that the thermally responsive features of these compounds are due to conformation changes upon altering the temperature of the solution and thus determine the communication between the phosphorus center and the conjugated backbones (i.e., the σ^*−π^* interaction).

In addition to the thermally responsive features in solution, the crystals of the new phospholium compounds also exhibit interesting mechanically responsive features (Figure 10a and Supporting Information). As general observation, the resulting powders from mechanical shearing of the crystals between two glass slides display a blue-shifted and broadened emission (**1a**, $\Delta\lambda_{em}$ = −3 nm; **1b**, $\Delta\lambda_{em}$ = −3 nm; **1c**, $\Delta\lambda_{em}$ = −2 nm; **2b**,

dx.doi.org/10.1021/ic2026335 | Inorg. Chem. 2012, 51, 2669−2678

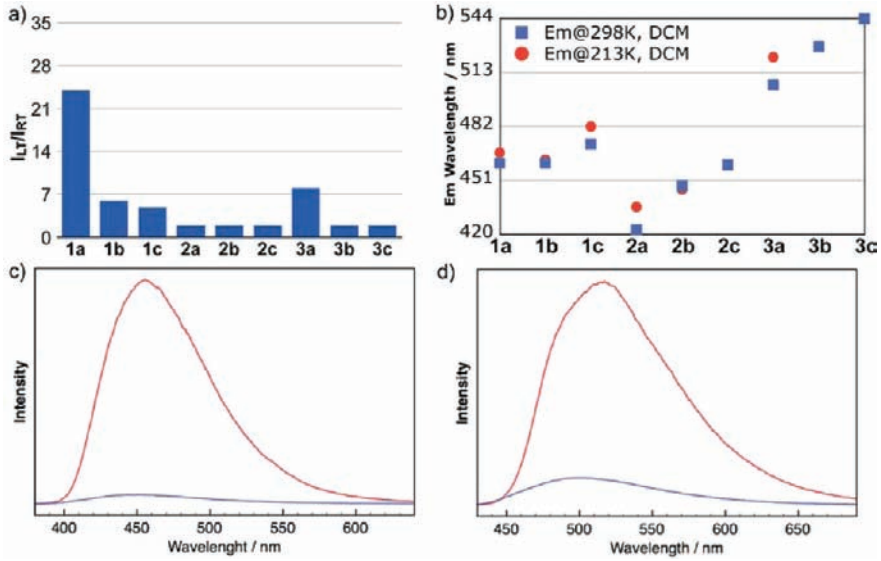

Figure 9. (a) Emission of **1**, **2**, and **3** series in CH_2Cl_2 (10^{-5} M) at room temperature (RT) and −60 °C (LT). (b) Emission wavelengths of the **1**, **2**, and **3** series in CH_2Cl_2 (10^{-5} M) at room temperature (blue circle) and −60 °C (red circle). (c and d) Emission spectra of **1a** and **3a** in CH_2Cl_2 (10^{-5} M) at room temperature (blue) and −60 °C (red).

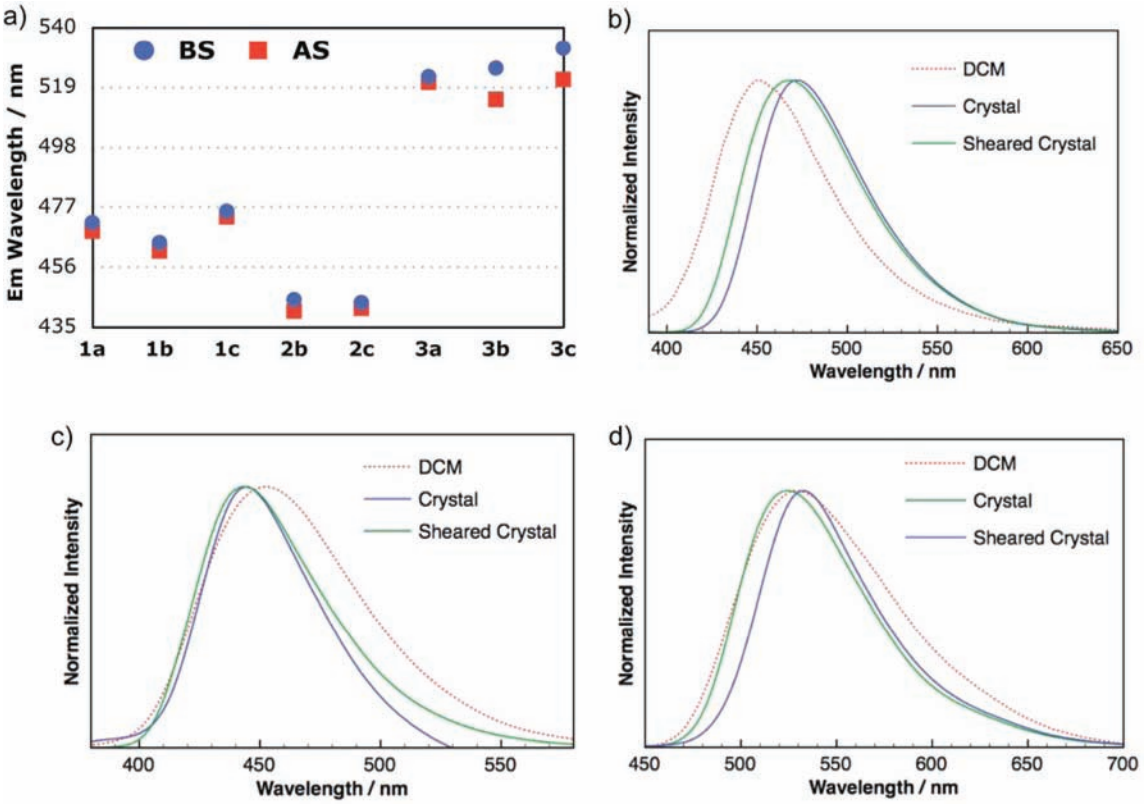

Figure 10. (a) Emission of the crystal phase of the **1**, **2**, and **3** series (BS, before shearing; AS, after shearing). (b, c, and d) Emission spectra of **1a**, **2c**, and **3c** under different conditions.

$\Delta\lambda_{em}$ = −4 nm; **2c**, $\Delta\lambda_{em}$ = −2 nm; **3a**, $\Delta\lambda_{em}$ = −2 nm; **3b**, $\Delta\lambda_{em}$ = −9 nm; **3c**, $\Delta\lambda_{em}$ = −11 nm). This mechanically responsive emission shift is believed to be the result of formation of different conformational isomers upon the mechanical force. In particular, crystals and sheared crystals of **2c** display blue-shifted emission compared with solution emission (Figure 10c), which further supports that comformation changes play an important role in this mechanical response. However, from the available data the intermolecular interaction changes, particularly for **1c** and **3c** with the observed $\pi-\pi$ stacking in the solid state, can also not fully be ruled out.

Interestingly, the sum of the emissions of the crystal and sheared crystal phases of **2b**, **3b**, and **3c** is very similar to the broad emission of these compounds in solution (Figure 10d

dx.doi.org/10.1021/ic2026335 | *Inorg. Chem.* 2012, 51, 2669−2678

and Supporting Information), which further points to the altered photophysics being based on conformation changes.

Theoretical Studies. The experimental results obtained in the context of this structure−property study suggest that the communication between the phosphorus center and the π-conjugated backbones ($\sigma^*-\pi^*$ coupling and inductive effect) is a crucial element of the dynamic structural features. Therefore, we evaluated the Mulliken charges on the phosphorus center for different conformations in order to further solidify the nature of the stimuli-responsive photophysical properites. Both "open" and "closed" conformations (Figure 11) of the **1**, **2**, and **3** series compounds were chosen as qualitative model isomers and subsequently optimized using DFT calculations (B3LYP/6-31G(d), PCM; solvent = CH_2Cl_2). Where applicable, X-ray diffraction data were used as input for the calculations. Indeed, the different conformations result in a noticeable change in the Mulliken charges at the P center (Figure 11), which clearly supports an altered electronic communication between the phosphorus center and the π-conjugated backbones. Besides, the theoretical calculations also show that the different molecular conformations can effectively change both LUMO and HOMO energy levels (Supporting Information) and can thus explain the thermally responsive emission in the solutions.

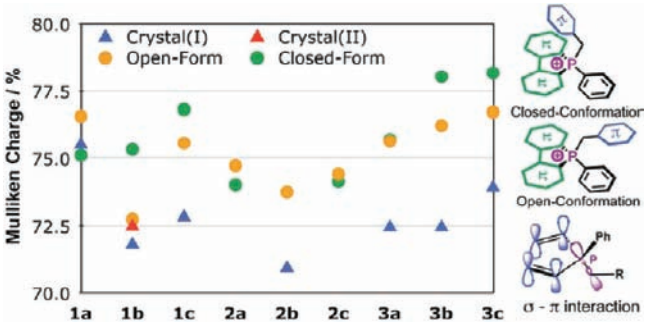

Figure 11. Mulliken charge of the phosphorus atom in the **1**, **2**, and **3** series for the different conformations.

Futhermore, the intermolecular effects on the stimuli-responsive behavior of the system were evaluated based on DFT calculations (B3LYP/6-31G(d), PCM; solvent = CH_2Cl_2) using the X-ray diffraction data for the dimeric structures of **1a**−**c** and **3a**−**c** (see Supporting Information). Although the two isomers of **1b** show very similar HOMO and LUMO energies (**1b**-*closed*, E_{HOMO} = −6.61 eV and E_{LUMO} = −2.63 eV; **1b**-*open*, E_{HOMO} = −6.60 eV and E_{LUMO} = −2.64 eV), the dimer of **1b**-*open* (dimer-open, E_{LUMO} = 3.86 eV) shows a smaller HOMO−LUMO gap compared to the dimer of **1b**-*closed* (dimer-closed, $E_{HOMO-LUMO}$ = 3.96 eV), which is consistent with the stronger $\pi-\pi$ stacking observed in the crystal of **1b**-*closed*.[10] Moreover, the HOMO and LUMO energy levels of the dimer of **3b** (E_{HOMO} = −6.61 eV, E_{LUMO} = −3.38 eV) are very similar to its monomer (E_{HOMO} = −6.65 eV, E_{LUMO} = −3.21 eV) and consistent with the low degree of $\pi-\pi$ stacking observed in the solid state. By contrast, the HOMO and LUMO energy levels of the dimer structures of **1a** (E_{HOMO} = −6.13 eV, E_{LUMO} = −2.61 eV), **1c** (E_{HOMO} = −6.99 eV, E_{LUMO} = −3.22 eV), **3a** (E_{HOMO} = −6.69 eV, E_{LUMO} = −3.43 eV), and **3c** (E_{HOMO} = −6.73 eV, E_{LUMO} = −3.38 eV) are very different from their corresponding monomers (**1a** E_{HOMO} = −6.28 eV and E_{LUMO} = −2.74 eV; **1c** E_{HOMO} = −6.71 eV and E_{LUMO} = −2.78 eV; **3a** E_{HOMO} = −6.50 eV and E_{LUMO} = −3.24 eV; **3b** E_{HOMO} = −6.65 eV and E_{LUMO} = −3.21 eV; **3c** E_{HOMO} = −6.48 eV and E_{LUMO} = −3.04 eV). Moreover, electronic coupling was exclusively observed between the π-conjugated scaffolds in the **1c** dimer (Figure 12b). Furthermore, TD-DFT calculations cleary support the potential for intermolecular charge transfer between the electron-rich trimethoxybenzyl group (HOMO) and the dimeric cores (LUMO) in **1a** and **3a** (Figure 12a, see Supporting Information). On the basis of the theoretical calculations, it is clear that both intermolecular charge transfer and dimerization in the excited state can contribute the red-shifted emission in the crystals.

CONCLUSION

We reported a series of new phospholium compounds whose dynamic structural features can be controlled via the different electronic nature of the substituted benzyl groups at the phosphorus center. Unlike in known phosphole/phospholium derivatives, this unique feature induces aggregation-induced enhanced emission (AIEE) due to restricted intramolecular rotation in the solid state. As a new molecular design concept, the structural dynamics can also endow this system with external-stimuli (temperature and mechanical force) responsive photophysics. The experimental data show that the $\sigma^*-\pi^*$ interaction can offer about 10 nm emission shift at low concentrations in solutions, which is quite efficient considering the small contribution of the phosphorus center. In the solid state, only the **3** series with a larger conjugated head exhibits a relatively strong mechanically responsive emission, indicating that the intermolecular interactions also play an important role due to the restricted conformation changes. Theoretical studies

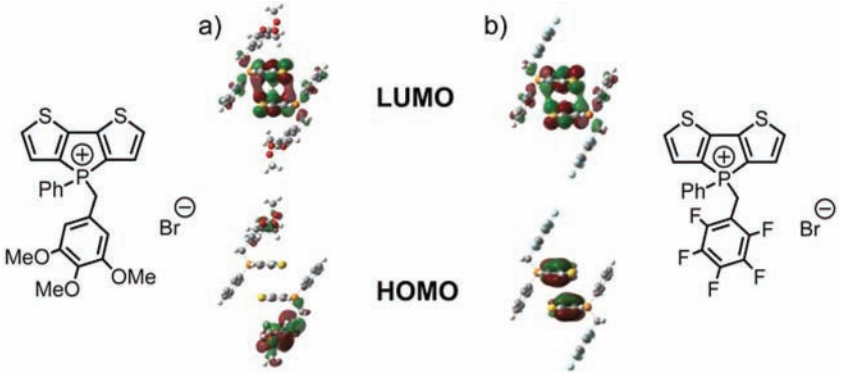

Figure 12. Molecular orbitals of **1a** (a) and **1c** (b) using X-ray diffraction data as input.

dx.doi.org/10.1021/ic2026335 | Inorg. Chem. 2012, 51, 2669−2678

further confirmed that both intramolecular conformation changes and intermolecular interactions (excimer and charge transfer) changes play an important role in this responsive emission as they are integral for the phosphole-typical $\sigma^*-\pi^*$ interaction that determines the overall photophysics of the system. More importantly, the thermally responsive hyperchromic shift and red-shifted emission are comparable to chemical modification of the phosphorus center of the corresponding systems reported before. These external-responsive features thus make the new phospholium materials promising candidates for a variety of sensing/biosensing applications.

■ ASSOCIATED CONTENT

Supporting Information

Additional ^{1}H, ^{31}P, VC/VT, and 2D NMR data, TD-DFT data, photophysical data, CIF files of all structures determined by X-ray crystallography, and intermolecular packing interactions of all crystallographically characterized compounds. This material is available free of charge via the Internet at http://pubs.acs.org. The CIF files were also deposited with the Cambridge Crystallographic Data center (CCDC), and CCDC codes 847303, 847304, 847305, and 847306 were allocated. These data are available without cost at www.ccdc.cam.ac.uk/conts/retrieving.html or from the CCDC, 12 Union Road, Cambridge CB2 IEZ, United Kingdom; fax: +44(0)1223−336033; e-mail: deposit@ccdc.cam.ac.uk.

■ AUTHOR INFORMATION

Corresponding Author

*E-mail: thomas.baumgartner@ucalgary.ca.

Notes

The authors declare no competing financial interest.

■ ACKNOWLEDGMENTS

Financial support by NSERC of Canada and the Canada Foundation for Innovation (CFI) is gratefully acknowledged. We also thank Alberta Ingenuity now part of Alberta Innovates-Technology Futures for a New Faculty Award (T.B.) and a graduate scholarship (Y.R.) as well as Talisman Energy for a graduate scholarship (Y.R.). The authors thank Prof. C. P. Berlinguette for access to the fluorescence instrument.

■ REFERENCES

(1) (a) Mercier, L. G.; Piers, W. E.; Parvez, M. *Angew. Chem., Int. Ed.* **2009**, *48*, 6108−6111. (b) Caruso, A. Jr.; Tovar, J. D. *Org. Lett.* **2011**, *13*, 3106−3109. (c) Wakamiya, A.; Mori, K.; Yamaguchi, S. *Angew. Chem., Int. Ed.* **2007**, *46*, 4273−4276. (d) Yamaguchi, S.; Akiyama, S.; Tamao, K. *J. Am. Chem. Soc.* **2001**, *123*, 11372−11375. (e) Elbing, M.; Bazan, G. C. *Angew. Chem., Int. Ed.* **2008**, *47*, 834−838.

(2) (a) Yamaguchi, S.; Tamao, K. *J. Chem. Soc., Dalton Trans.* **1998**, 3693−3702. (b) Zhan, X.; Barlow, S.; Marder, S. R. *Chem. Commun.* **2009**, 1948−1955. (c) Zhan, X.; Risko, C.; Amy, F.; Chan, C.; Zhao, W.; Barlow, S.; Kahn, A.; Brédas, J.-L.; Marder, S. R. *J. Am. Chem. Soc.* **2005**, *127*, 9021−9029. (d) Yamaguchi, S.; Xu, C.; Tamao, K. *J. Am. Chem. Soc.* **2003**, *125*, 13662−13663. (e) Xu, C.; Wakamiya, A.; Yamaguchi, S. *J. Am. Chem. Soc.* **2005**, *127*, 1638−1639.

(3) (a) Fukazawa, A.; Yamaguchi, S. *Chem. Asian J.* **2009**, *15*, 1386−1400. (b) Baumgartner, T; Réau, R. *Chem. Rev.* **2006**, *106*, 4681−4727. (correction: *Chem. Rev.* **2007**, *108*, 303). (c) Dillon, K. B.; Mathey, F.; Nixon, J. F. *Phosphorus: The Carbon Copy*; Wiley: New York, 1998. (d) Mathey, F. *Phosphorus-Carbon Heterocyclic Chemistry: The Rise of a New Domain*; Pergamon Press: Amsterdam, 2001. (e) Linder, T.; Sutherland, T. C.; Baumgartner, T. *Chem.—Eur. J.* **2010**, *16*, 7101−7105. (f) Durben, S.; Baumgartner, T. *Inorg. Chem.* **2011**, *50*, 6823−6836. (g) Durben, S.; Baumgartner, T. *Angew. Chem., Int. Ed.* **2011**, *50*, 7948−7952.

(4) (a) Curtis, M. D.; Cao, J.; Kampf, J. W. *J. Am. Chem. Soc.* **2004**, *126*, 4318−1055. (b) Kim, E.-G.; Coropceanu, V.; Gruhn, N. E.; Sánchez-Carrera, R. S.; Snoeberger, R.; Matzger, A. J.; Brédas, J.-L. *J. Am. Chem. Soc.* **2007**, *129*, 13072−13081. (c) Suzuki, Y.; Okamoto, T.; Wakamiya, A.; Yamaguchi, S. *Org. Lett.* **2008**, *10*, 3393−3396. (d) Amir, E.; Rozen, S. *Angew. Chem., Int. Ed.* **2005**, *44*, 7374−7378. (e) Barbarella, G.; Favaretto, L.; Zambianchi, M.; Pudova, O.; Arbizzani, C.; Bongini, A.; Mastragostino, M. *Adv. Mater.* **1998**, *10*, 551−554. (f) Tedesco, E.; Sala, F. D.; Favaretto, L.; Barbarella, G.; Albesa-Jové, D.; Pisignano, D.; Gigli, G.; Cingolani, R.; Harris, K. D. M. *J. Am. Chem. Soc.* **2003**, *125*, 12277−122783.

(5) (a) Jäkle, F. *Chem. Rev.* **2010**, *110*, 3985−4022. (b) Wade, C. R.; Broomsgrove, A. E. J.; Aldridge, S.; Gabbaï, F. P. *Chem. Rev.* **2010**, *110*, 3958−3984. (c) Hudson, Z, M.; Wang, S. *Acc. Chem. Res.* **2009**, *42*, 1548−1596.

(6) (a) Chu, T.-Y.; Lu, J.; Beaupré, S.; Zhang, Y.; Pouliot, J.-R.; Wakim, S.; Zhou, J.; Leclerc, M.; Li, Z.; Ding, J.; Tao, Y. *J. Am. Chem. Soc.* **2011**, *125*, 4250−4253. (b) Hou, J.; Chen, H.-Y.; Zhang, S.; Li, G.; Yang, Y. *J. Am. Chem. Soc.* **2008**, *130*, 16144−16145. (c) Sohn, H.; Sailor, J. M.; Magde, D.; Trogler, W. C. *J. Am. Chem. Soc.* **2003**, *125*, 3821−3830.

(7) (a) Matano, Y.; Saito, A.; Fukushima, T.; Tokudome, Y.; Suzuki, F.; Sakamaki, D.; Kaji, H.; Ito, A.; Tanaka, K.; Imahori, H. *Angew. Chem., Int. Ed.* **2011**, *50*, 8016−8020. (b) Romero-Nieto, C.; Durben, S.; Kormos, I. M.; Baumgartner, T. *Adv. Funct. Mater.* **2009**, *19*, 3625−3631. (c) Fadhel, O.; Gras, M.; Lemaitre, N.; Deborde, V.; Hissler, M.; Geffroy, B.; Réau, R. *Adv. Mater.* **2009**, *21*, 1261−1265. (d) Tsuji, H.; Sato, K.; Sato, Y.; Nakamura, E. *J. Mater. Chem.* **2009**, *19*, 3364−3366. (e) Su, H.-C.; Fadhel, O.; Yang, C.-J.; Cho, T.-Y.; Fave, C.; Hissler, M.; Wu, C.-C.; Réau, R. *J. Am. Chem. Soc.* **2006**, *128*, 983−995. (f) Fave, C.; Cho, T.-Y.; Hissler, M.; Chen, C.-W.; Luh, T.-Y.; Wu, C.-C.; Réau, R. *J. Am. Chem. Soc.* **2003**, *125*, 9254−9255.

(8) Xiao, K.; Liu, Y.; Qi, T.; Zhang, W.; Wang, F.; Gao, J.; Qiu, W.; Ma, Y.; Cui, G.; Chen, S.; Zhan, X.; Yu, G.; Qin, J.; Hu, W.; Zhu, D. *J. Am. Chem. Soc.* **2005**, *127*, 13281−13286.

(9) (a) Ren, Y.; Baumgartner, T. *J. Am. Chem. Soc.* **2011**, *133*, 1328−1340. (b) Dienes, Y.; Durben, S.; Kárpáti, T.; Neumann, T.; Englert, U.; Nyulászi, L.; Baumgartner, T. *Chem.—Eur. J.* **2007**, *13*, 7487−7500. (c) Ren, Y.; Baumgartner, T. *Chem.—Asian J.* **2010**, *5*, 1918−1929. (d) Baumgartner, T.; Neumann, T.; Wirges, B. *Angew. Chem., Int. Ed.* **2004**, *43*, 6197−6201. (e) Durben, S.; Dienes, Y.; Baumgartner, T. *Org. Lett.* **2006**, *8*, 5893−5893. (f) Dienes, Y.; Eggenstein, M.; Kárpáti, T.; Sutherland, T. C.; Nyulászi, L.; Baumgartner, T. *Chem.—Eur. J.* **2008**, *14*, 9878−9889. (g) Ren, Y.; Dienes, Y.; Hettel, S.; Parvez, M.; Hoge, B.; Baumgartner, T. *Organometallics* **2009**, *28*, 734−740. (h) Romero-Nieto, C.; Kamada, K.; Cramb, D. T.; Merino, S.; Rodríguez-López, J.; Baumgartner, T. *Eur. J. Org. Chem.* **2010**, *27*, 5225−5231. (i) Romero-Nieto, C.; Merino, S.; Rodríguez-López, J.; Baumgartner, T. *Chem. – Eur. J.* **2009**, *15*, 4135−4145. (j) Dienes, Y.; Eggenstein, M.; Neumann, T.; Englert, U.; Baumgartner, T. *Dalton Trans.* **2006**, 1424−1433.

(10) Ren, Y.; Kan, W. H.; Henderson, M. A.; Bomben, P. G.; Berlinguette, C. P.; Thangadurai, V.; Baumgartner, T. *J. Am. Chem. Soc.* **2011**, *133*, 17014−17026.

(11) Concentration NMR studies could not be carried out for **3b** and **3c** due to their low solubility in $CDCl_3$ at 298 K.

(12) Two crystal isomers of **1b** have been reported by our group (see ref 10). For compounds of **1a** (ethyl acetate or $CHCl_3$), **2b**, and **2c**, X-ray data were not good enough to get acceptable metric parameters. However, the crystals were used for photophysical measurements and theoretical calculations.

(13) (a) Hong, Y.; Lam, J. W. Y.; Tang, B. Z. *Chem. Commun.* **2009**, 4332−4353. (b) Hong, Y.; Lam, J. W. Y.; Tang, B. Z. *Chem. Soc. Rev.* **2011**, *40*, 4332−4353.

(14) Würthner, F.; Kaiser, T. E.; Saha-Möller, C. R. *Angew. Chem., Int. Ed.* **2011**, *50*, 3376−3410.